Intermetallics 17 (2009) 886–893

Contents lists available at ScienceDirect

Intermetallics

journal homepage: www.elsevier.com/locate/intermet

Microstructural evolution of spinodally formed $Fe_{35}Ni_{15}Mn_{25}Al_{25}$

Ian Baker [a,*], R.K. Zheng [b], David W. Saxey [b], Satoko Kuwano [b], Markus W. Wittmann [a], Johnathan A. Loudis [a], K.S. Prasad [b], Zongwen Liu [b], Ross Marceau [b], P.R. Munroe [c], Simon P. Ringer [b]

[a] Thayer School of Engineering, Dartmouth College, Hanover, NH 03755, USA
[b] Australian Key Centre for Microscopy and Microanalysis, The University of Sydney, Sydney, NSW 2006, Australia
[c] Electron Microscope Unit, University of New South Wales, Sydney, NSW, Australia

ARTICLE INFO

Article history:
Received 22 September 2008
Accepted 16 March 2009
Available online 9 May 2009

Keywords:
Atom probe
Diffraction electron

ABSTRACT

The microstructural evolution of a b.c.c.-based, spinodally formed alloy $Fe_{35}Ni_{15}Mn_{25}Al_{25}$ has been studied as a function of annealing time at 550 °C using atom probe tomography and transmission electron microscopy, including energy-filtered imaging. The sizes, crystal structures, orientation relationships and compositions of the phases present were determined as a function of annealing time. The hardness showed complicated behavior as a function of annealing time, consisting of initial hardening, followed by softening and finally, by a rapid hardening behavior. The hardness is controlled both by the coarsening of the spinodally formed phases, and the precipitation and growth of β-Mn structured particles.

1. Introduction

Starting with the discovery of the spinodally formed alloy $Fe_{30}Ni_{20}Mn_{25}Al_{25}$ (in at. %), several b.c.c.-based spinodally formed alloys have been discovered in the Fe–Ni–Mn–Al system [1,2,17,31–33,37,39]. The parent phase for this spinodal transformation is believed to be a B2 (ordered b.c.c.) phase [17]. The alloys typically consist of coherent, alternating rods or platelets of b.c.c. and B2 phases aligned along ⟨100⟩ directions [17]. This type of microstructure is characteristic of a spinodal decomposition in a b.c.c.-alloy in which the phases are coherent. The wavelengths associated with the decomposition range from 10 to 120 nm depending on the alloy composition [39]. Interestingly, plastic deformation at room temperature, at least in $Fe_{30}Ni_{20}Mn_{25}Al_{25}$, is accommodated by the glide of paired a/2 ⟨111⟩ dislocations [32].

The strengths of the spinodally formed Fe–Ni–Mn–Al alloys are comparable to the strongest maraged aircraft steels and hardest bearing steels, but they possess a better strength-to-weight ratio, and the high aluminum content contributes to oxidation resistance. A survey of several as-cast Fe–Ni–Mn–Al spinodally formed alloys [39] showed that $Fe_{35}Ni_{15}Mn_{25}Al_{25}$ had the highest as-cast hardness at 534 ± 12 VPN. This alloy consisted of the usual alternating ordered and disordered b.c.c. rods, but the B2 rods displayed regions of $L2_1$ ordering (a further ordering of the B2 structure). Annealing at 625 °C for 115 h appeared to decrease the $L2_1$ ordering, but led to both a substantial increase in the spinodal wavelength from ~10 nm to 50 nm and to the formation of (Fe,Mn)-rich precipitates that were 100 nm wide and 0.5–1 μm long [39]. Similar precipitates have been analyzed in some detail in the related spinodally formed alloy $Fe_{30}Ni_{20}Mn_{25}Al_{25}$ [33], in which the precipitates were shown to have a clear relationship with the matrix.

In an earlier study [17], it was shown that annealing $Fe_{30}Ni_{20}Mn_{25}Al_{25}$ at 550 °C – the temperature at which the greatest hardness increase occurred – led to a substantial (50%) monotonic increase in hardness for annealing times up to 96 h. In this paper, we examine the effect of annealing at 550 °C for times up to 72 h on the hardness of the alloy $Fe_{35}Ni_{15}Mn_{25}Al_{25}$, and investigate the accompanying changes in microstructure using both atom probe tomography (APT) and transmission electron microscopy (TEM), including energy dispersive X-ray spectrometry (EDS) and energy-filtered imaging (EFTEM).

2. Experimental

An ingot of $Fe_{35}Ni_{15}Mn_{25}Al_{25}$ alloy was prepared by arc-melting the constituent elements of >99.9% purity in a water-cooled copper mold under argon. The ingot was melted four times and flipped between meltings to ensure adequate mixing. Analysis using a Cameca SX50 electron probe microanalyzer confirmed that final compositions were all within 0.4 at. % of the nominal values.

* Corresponding author.
E-mail address: Ian.Baker@Dartmouth.edu (I. Baker).

0966-9795/$ – see front matter © 2009 Elsevier Ltd. All rights reserved.
doi:10.1016/j.intermet.2009.03.016

The alloy was annealed at 550 °C in air for up to 72 h, followed by air cooling. As noted above, such annealing has previously been shown to markedly increase both the hardness and yield strength [17].

Hardness measurements were performed at room temperature using a Leitz MINIload tester with a Vickers-type indenter using a 200 g load and a 12 s drop time. Reported values are the average of at least 5 measurements.

Transmission electron microscopy was used to characterize the microstructure. Small samples ($0.4 \times 1 \times 3$ mm) were first cut with a water-cooled diamond saw and mechanically ground with 1 μm diamond encrusted paper. These ground wedges, were supported by copper grids and thinned using a Gatan precision ion polishing system. The specimens were examined using both a 120 kV Philips CM12 TEM and a 300 kV JEOL 3000F TEM equipped with EDS and a Gatan electron energy loss spectroscopy (EELS) system, incorporating a post-column Gatan Image Filter for energy filtered transmission electron microscopy.

Atom probe tomography (APT) was used to study the very fine scale phase elemental partitioning between the phases. Since the APT uses a mass spectrometer it is straightforward to distinguish between Fe, Ni, Mn and Al, except for the overlap of ^{58}Fe and ^{58}Ni. However, this overlap can usually be accounted for, since the natural abundance of the isotopes is known. In fact, the natural abundance of ^{58}Fe is so low that it can be ignored. Another important aspect of APT analysis to consider is the different evaporation fields of the elements at the specimen surface: elements with low evaporation field may evaporate between the evaporation pulses, and thus not be detected, resulting in an underestimated measured concentration. A pulse fraction (pulse voltage over standing voltage) of 20%, and low specimen temperature of 80 K was used to minimize this effect.

Specimens for APT were prepared from square-sectioned blanks ($0.4 \times 0.4 \times 10$ mm), cut using a diamond saw, electropolished using standard procedures, and examined using an Imago local electrode atom probe, which provides high-speed data acquisition over a large spatial and angular field of view.

3. Results

Fig. 1 shows the hardness dependence on annealing time at 550 °C. Unlike the related alloy $Fe_{30}Ni_{20}Mn_{25}Al_{25}$, which showed a monotonic increase in hardness with increasing annealing time at 550 °C [17], $Fe_{35}Ni_{15}Mn_{25}Al_{25}$ shows an initial increase in hardness for short annealing times, which then declines slightly for times up to 2 h. For a slightly longer annealing time (2 h) the hardness falls more rapidly, after which it is independent of time for times up to ~40 h. Finally, for longer annealing times (70 h), the hardness increases dramatically from 540 VPN to more than 660 VPN.

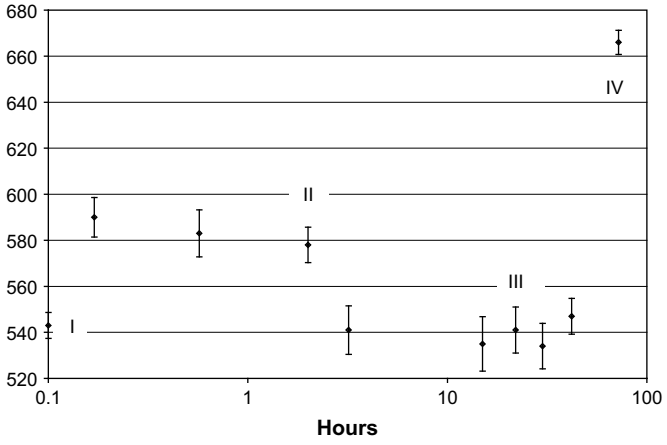

Fig. 1. Room temperature hardness dependence of Fe–15Ni–25 Mn–25Al on annealing time at 550 °C. Specimens from the as-cast material (I) and for three different annealing times (II – 2 h; III – 22 h; IV – 72 h) were examined using TEM and APT.

As noted above, previous TEM studies [39] showed that $Fe_{35}Ni_{15}Mn_{25}Al_{25}$ has a periodic coherent microstructure, suggesting formation by spinodal decomposition. The interconnected nature of the microstructure is clear in the TEM images, see Fig. 2(a–d). The formation of very large lenticular precipitates 1–2 μm long, as previously found in $Fe_{30}Ni_{20}Mn_{25}Al_{25}$ [17], is also clearly apparent in the 72 h annealed specimen, see Fig. 2(d).

The very strong elemental partitioning between the phases, previously noted in $Fe_{30}Ni_{20}Mn_{25}Al_{25}$ [17], is evident in the EFTEM images. Fig. 3 shows Fe, Ni, Mn, Al maps of the 2 h annealed specimen filtered using M-edges for Fe, Ni and Mn, and an L-edge for Al. It is clear that Ni co-segregates with Al and that Fe co-segregates with Mn. It is worth noting the strong ordering tendencies of Ni and Al, and the high solubility of Mn in both Fe and Ni. These factors can provide enough flexibility in elemental segregation to allow for close lattice matching between the two phases. Such segregation during spinodal decomposition involves a very low coherency strain barrier and, hence, can proceed much more rapidly than phase separation by nucleation and growth [7].

The initially insuppressible concentration waves, which define the beginnings of a regular, periodic, and often interconnected array of two coherent phases, is characteristic of the spinodal decomposition of a solid solution [8,9]. The orientation of concentration waves, i.e., the spinodal phases, is determined by the elastic anisotropy of the lattice, so it favors the weak cube directions of low elastic anisotropy [8]. High resolution TEM (HRTEM) was used to determine the spinodal phase orientations in the $Fe_{35}Ni_{15}Mn_{25}Al_{25}$ specimens. Both the spinodal decomposition waves and crystallographic lattices can be seen simultaneously in the HRTEM images shown in Figs. 4(a–d). The insets are the corresponding fast Fourier transform (FFT) patterns of lattices, which indicate the direction of the lattices. It is clear that the spinodal decomposition propagates along ⟨100⟩ directions, as previously reported [17].

The wavelength (λ) and amplitude (A) are the two parameters most commonly used to describe spinodal alloys [10,12–14,18–20]. The average spinodal wavelengths in the current alloy were determined by measuring FFT spots, see Figs. 4(a–d). The results are summarized in Table 1. It is clear from the micrographs and Table 1 that the wavelength increases monotonically with increasing ageing time.

Figs. 2(e–h and i–l) shows selected area electron diffraction patterns (SADPs) taken along [001] and [101], respectively, of both the as-cast alloy and after 2 h, 22 h and 72 h anneals. The BF images in Fig. 2, which were taken along ⟨100⟩, together with the diffraction patterns again confirm that the spinodally formed microstructure is aligned along ⟨100⟩. The SADPs from the 2 h annealed specimen taken along both [100] and [101] clearly display the presence of a B2 structure, see Figs. 2(f, j) – the b.c.c. diffraction spots are coincident with the fundamental reflections of the B2 structure. Additional diffraction spots are present in [101] SADPs from both the as-cast and 22 h annealed specimens, as shown in Figs. 2(i, k) confirming the presence of $L2_1$ ordering, as previously observed for this alloy in the as-cast state [39]. It is not immediately clear why $L2_1$ ordering was found in the as-cast material and after the 22 h anneal, but not after the 2 h or 72 h anneals. It was previously noted that the $L2_1$ ordering decreased after a 112 h anneal at 615 °C [39]. One possible explanation is the additional ($L2_1$) ordering reflects compositional heterogeneity. Long streaks through {110} along [110] are also present in the [001] diffraction patterns of the as-cast and 22 h annealed specimens, see Figs. 2(e, g). The origin of this streaking is